Factors responsible for the limited inland extent of sand deposits on Leyte Island during 2013 Typhoon Haiyan

Watanabe, M.; Bricker, Jeremy; Goto, K.; Imamura, F.

DOI
10.1002/2016JC012023

Publication date
2017

Document Version
Final published version

Published in
Journal Of Geophysical Research-Oceans

AGU PUBLICATIONS

JGR

Journal of Geophysical Research: Oceans

RESEARCH ARTICLE

10.1002/2016JC012023

Factors responsible for the limited inland extent of sand deposits on Leyte Island during 2013 Typhoon Haiyan

M. Watanabe[1], J. D. Bricker[2,3], K. Goto[2], and F. Imamura[2]

[1]School of Engineering, Tohoku University, Sendai, Japan, [2]International Research Institute of Disaster Science, Tohoku University, Sendai, Japan, [3]Department of Hydraulic Engineering, Faculty of Civil Engineering and Geosciences, Delft University of Technology, Delft, Netherlands

Key Points:
- Flow velocity over land due to waves and storm surge is small, so that maximum inland extent of storm deposit is short
- The distribution of sand deposits is heavily affected by wave intensity and the roughness coefficient over land
- Useful proxies for identifying storm deposits are their limited inland extent and the presence of multiple layers

Correspondence to:
M. Watanabe.
masashi.watanabe.r3@dc.tohoku.ac.jp

Citation:
Watanabe, M., J. D. Bricker, K. Goto, and F. Imamura (2017), Factors responsible for the limited inland extent of sand deposits on Leyte Island during 2013 Typhoon Haiyan, *J. Geophys. Res. Oceans*, *122*, doi:10.1002/2016JC012023.

Received 4 JUN 2016
Accepted 25 FEB 2017
Accepted article online 2 MAR 2017

Abstract Previous geological studies suggest that the maximum inland extent of storm-induced sand deposits is shorter, but their thickness is larger, than those of tsunami-induced sand deposits. However, factors that determine the maximum extent and thickness of storm deposits are still uncertain. We conducted numerical simulations of storm surge, waves, and sediment transport during Typhoon Haiyan in order to understand the distribution and sedimentary processes responsible for storm deposits. Numerical results showed that wave-induced currents slightly offshore were strong, but attenuated rapidly in the inland direction after wave breaking. Therefore, sediments were not transported far inland by waves and storm surge. Consequently, the maximum inland extent of storm deposits was remarkably shorter than the inland extent of inundation. We also revealed that vegetation (roughness coefficient) and typhoon intensity greatly affect the calculation of maximum extent and thickness distribution of storm deposits. As the duration of wave impact on a coast is relatively long during a storm (hours, compared to minutes for a tsunami), sediments are repeatedly supplied by multiple waves. Therefore, storm deposits tend to be thicker than tsunami deposits, and multiple layers can form in the internal sedimentary structure of the deposits. We infer that limitation of the sand deposit to within only a short distance inland from the shoreline and multiple layers found in a deposit can be used as appropriate identification proxies for storm deposits.

1. Introduction

Understanding the recurrence interval and size of past typhoons is important in order to better assess regional hazard risk. In particular, if sandy deposits can be identified as being of storm origin (as opposed to tsunami origin), these deposits can help identify the characteristics of storms that affected the area in the past. Such information is very useful for investigating historical and prehistoric storm events throughout the world.

Recently, sandy storm deposits, which are defined here as sandy deposits formed by storm surge and/or waves, have been reported in many regions, and their sedimentary features have been a topic of research [e.g., *Hawkes and Horton*, 2012; *Phantuwongraj et al*., 2013; *Shaw et al*., 2015; *Williams* 2013, 2015]. It has been pointed out that sedimentary features of storm deposits are similar to those of tsunami deposits [e.g., *Goff et al*., 2004*; Goto et al*., 2015*; Kain et al*., 2014*; Phantuwongraj and Choowong*, 2012]. However, criteria to distinguish storm deposits from tsunami deposits are not well-established [e.g., *Goff et al*., 2012]. *Morton et al*. [2007] reported that storm deposits have more layers and are thicker (25–200 cm) than tsunami deposits, because storm deposits are formed by multiple waves [*Morton et al*., 2007]. In fact, the maximum sediment thickness of tsunami deposits was generally ~30 cm in the case of the 2011 Tohoku-oki tsunami [e.g., *Goto et al*., 2014] and 50 cm in case of the 2004 Indian Ocean tsunami [*Szczuciński*, 2012], although a tsunami deposit with 150 cm in thickness was reported [*Peters and Jaffe*, 2010] as an exceptional case.

It is likely that the criteria proposed by *Morton et al*. [2007] are generally applicable to differentiate storm and tsunami deposits. However, it is still unclear whether these sedimentological differences are universal, because quantitative verification of sedimentary differences has not been thoroughly examined. Recently, the process of tsunami deposit formation has been investigated numerically [e.g., *Apotsos et al*., 2011; *Sugawara et al*., 2014], but no similar work has been performed for storm deposits.

From a hydraulic perspective, a principle difference between tsunamis and storm waves is wave period [e.g., *Goto et al*., 2009]. Tsunami wave period is several minutes to hours [e.g., *Nagai et al*., 2007]. Meanwhile,

storm wave period is several seconds to slightly greater than 20 s [*Goto et al*., 2009]. Some exceptions exist in case of storm events depending on topography. For example, surf beat, which is a long period fluctuation of sea level with a period on the order of minutes [e.g., *Sekimoto et al*., 1990], can be generated over a flat and shallow topography such as a reef.

After wave breaking, storm wave height quickly attenuates inland over the flat topography due to the short wave period [*Egashira et al*., 1985]. Therefore, it is likely that storm deposits may be formed near the shoreline but not further inland. On the other hand, storm surge during a passing typhoon could last as long as several hours [*The Ministry of Agriculture, Forestry and Fisheries*, 2015]. However, storm surge over a flat coastal plain often does not entail strong horizontal current speeds, as in the case of Hurricane Katrina's storm surge in Mississippi [*Dietrich et al*., 2011] or for the case of Typhoon Haiyan's storm surge in Tacloban [*Bricker et al*., 2014]. Therefore, the capacity of the storm surge to transport sediments may be small.

Qualitatively speaking, the maximum inland extent of sandy deposits formed by storms may be shorter than that formed by tsunamis due to the above mentioned hydraulic differences between tsunami and storm waves/surge. In fact, it is rare that sandy storm deposits are distributed several hundred meters inland [e.g., *Dawson et al*., 1991]. This hypothesis is further supported by a recent study of sandy storm deposits formed by Typhoon Haiyan, which struck Tacloban in the Philippines on 8 November 2013. *Abe et al*. [2015] revealed that the deposits were distributed only up to 130–180 m inland. This is only about 7.0–8.0% of the inland inundation distance (1400–3100 m). *Pilarczyk et al*. [2016] however, reported that some sandy storm deposits formed by Typhoon Haiyan were locally distributed up to 85% of the inundation limit in Leyte gulf. Therefore, distribution of storm deposits is complex, and local effects should be considered.

Contrary to storm deposits, the deposits formed by the 2004 Indian Ocean tsunami [e.g., *Jaffe et al*., 2006] and the 2011 Tohoku-oki tsunami [e.g., *Abe et al*., 2012] were distributed several kilometers inland, and reached close to the inundation limit. In fact, several previous studies identified specific paleoevents as tsunamis rather than storms based on the fact that the sand deposited by these events reached far beyond the possible inland limit of storm deposits [e.g., *Sawai et al*., 2009].

It is, however, still unclear whether differentiating tsunami and storm deposits based on the difference in maximum extent of sand deposition is always possible or not. In the case of sandy storm deposits formed during Typhoon Haiyan, it is also unclear why the maximum extent of storm deposits is significantly shorter (extends less far inland) than the inundation limit at the study sites by *Abe et al*. [2015]. Moreover, the factors (e.g., land conditions or wave conditions) that control the distribution and thickness of storm deposits should be explored.

In this study, we conducted numerical simulations of storm waves and surge plus sediment transport during Typhoon Haiyan to understand the formation process of sandy storm deposits and to examine the main factors that determine maximum extent and thickness of the sand layer. We further examined the sedimentological and hydraulic differences between sandy deposits left by storms and those left by tsunamis.

2. Study Area

In order to examine the process of storm deposit formation, it is necessary to verify not only the reproducibility of the wave field but also the distribution of the sand layer thickness. In this study, we selected towns south of Tacloban in the Philippines as our study area, where *Abe et al*. [2015] measured the thickness distribution of Typhoon Haiyan's storm deposits (Figure 1).

The Philippines is a tropical climate. The coast near Tacloban consists of beaches and sand dunes behind the shoreline. Further upland are cities, forests, and vegetation. On 8 November 2013, Typhoon Haiyan made landfall in the Philippines and killed more than 6000 people [*U.S. Agency for International Development*, 2014]. The maximum 10 min sustained wind speed and central pressure near Guiuan on 8 November, 3:40, 2013 (UTC +8 h) were 125 kt and 895 hPa, respectively [*Tajima et al*., 2014].

Bricker et al. [2014] conducted a numerical simulation of the wave field during Typhoon Haiyan. The maximum significant wave height reached up to 19 m off Eastern Samar and about 5 m near Tacloban. *Roeber and Bricker* [2015] reported that a destructive tsunami-like wave was generated by surf beat in Hernani, a town exposed to the open ocean, because wave breaking was generated over fringing reef topography

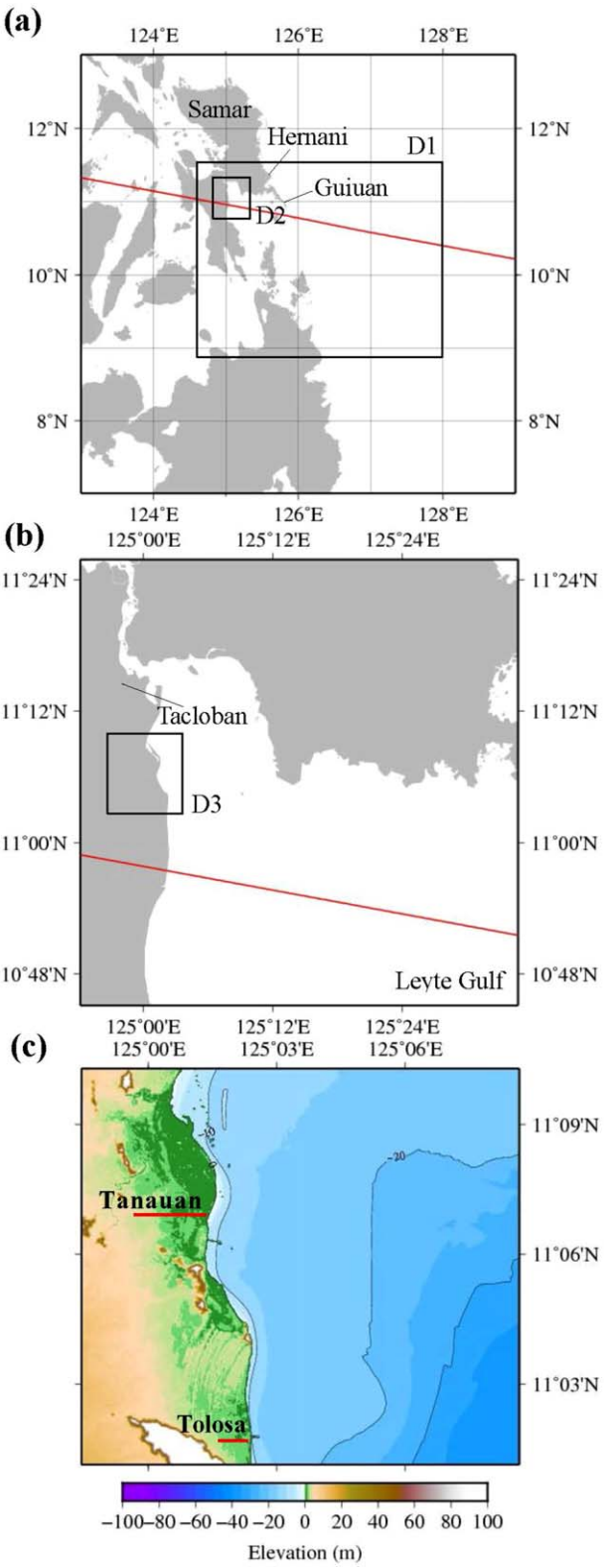

Figure 1. (a) Map of the first domain (D1). Location of the second domain (D2) is shown. Red line is the actual path of Typhoon Haiyan [*Japan Meteorological Agency*, 2013]. (b) Map of the second domain (D2). Location of the third domain (D3) is shown. (c) Map of the third domain. Locations of the Tanauan and Tolosa transects sampled by *Abe et al.* [2015] are shown.

and setup of the water surface oscillated with the incidence of large and small wave groups. However, the shallow San Pablo Bay fronting the study sites of Tanauan and Tolosa is a dissipative environment in which long-period wave motions should be less dominant.

Due to the storm waves and surge during Typhoon Haiyan, deposition of boulders [e.g., *May et al.*, 2015; *Switzer et al.*, 2014; *Mas et al.*, 2015; *Kennedy et al.*, 2016] and sand [*Abe et al.*, 2015; *Pilarczyk et al.*, 2016; *Tajima et al.*, 2016a] were reported. *Abe et al.* [2015] investigated the distribution of sandy deposits along two transects at Tolosa and Tanauan (Figure 1). They reported that the maximum inland extent of sand deposition was 130 m from the shoreline while the inundation extended 1400 m inland along the Tolosa transect. Along the Tanauan transect, the maximum inland extent of the sand layer was 180 m from the shoreline, while the inundation extended 3100 m inland. Along the Tanauan transect, *Abe et al.* [2015] measured a deposit of 80 cm thickness just behind the sand dune. However, this might be an overestimation because a portion of this deposit may be due to wind (T. Abe, personal communication). Field observations revealed that sand deposits near the inland distribution limit in each transect are composed of very fine sand, although further detailed grain-size measurements are required. In this study, we conducted numerical simulations of these two transects.

3. Methods

3.1. Numerical Model Used for the Parameter Study

In this study, we used Delft-3D/SWAN [*Deltares*, 2011] to calculate the wave field and sediment transport. Delft-3-D applied with one vertical layer implements the shallow water equations to calculate water elevation and current fields, then passes the numerical result to SWAN [*Deltares*, 2011]. SWAN calculates spectral parameters of the wave field via the conservation of wave action. Then, SWAN passes the numerical result for radiation stresses back to Delft-3-D, so that wave setup and the

mean current field induced by wave setup are calculated. Sediment transport due to both wave-induced orbital velocities and mean wave-setup-induced currents are also calculated by Delft-3-D [*Deltares*, 2011]. Using a similar numerical scheme, *Bricker et al*. [2014] modeled the wave field during Typhoon Haiyan and *Soria et al*. [2016] simulated wave fields during both Typhoon Haiyan and the typhoon that hit the same area in the year 1897. As shown by *Roeber and Bricker* [2015], there is a possibility that surf beat may have an effect on runup and damage along steep (reef-type) coasts, and that phase-averaged wave models such as SWAN cannot simulate this phenomenon well. However, previous works showed that storm surge along the gently sloping coasts of Tanauan and Tolosa could be simulated to match measurements well using only a phase-averaged wave model together with a hydrodynamics model [*Bricker et al*., 2014; *Mori et al*., 2014; *Takagi et al*., 2017; *Tajima et al*., 2016b], indicating that surf beat does not play a primary role here.

The data of the behavior of Typhoon Haiyan used in this calculation were created by using the method of *Bricker et al*. [2014]. The actual moving path and central pressure of the typhoon [*Japan Meteorological Agency*, 2013] was input into the parametric hurricane model of *Holland* [1980] for estimation of the air-pressure and wind fields. To account for asymmetry of these fields due to forward motion of the typhoon, the method was modified per *Fujii and Mitsuda* [1986]. Radius to maximum winds was estimated by using the empirical relation of *Quiring et al*. [2011].

Model resolution was 0.01° for domain D1, 0.002° for D2, and 0.0004° for D3 (Figure 1). Tides are included using the Global Tide database TPXO [*TPXO*, 2014] as a boundary condition of the first domain in the hydrodynamic model. Topography in domains 1 and 2 were created from SRTM data [*NASA*, 2014] while 5 m resolution topography created from field survey data [*Japan International Cooperation Agency*, 2014] was used in domain 3 for high-resolution inundation modeling. Bathymetry was from GEBCO [*IOC et al*., 2003]. The calculation time is 4 days from 6 to 9 November 2013. For 3 days from 6 to 9 November, the tide calculation was spun up. From 8 to 9 November, the wind and pressure fields were added to the input, for the calculation of storm surge and waves.

A movable sediment bed of 5 m in thickness was assumed to exist everywhere from the sea floor to the sand dunes. As we describe later, the calculated maximum erosion among all simulated cases in domain 3 is 4.9 m, less than the 5 m thickness assumed for the sediment bed, indicating that the assumed sediment bed thickness does not have an effect on the model result. According to *Abe et al*. [2015], the maximum inland extent of the sand layer is defined as the location where a sediment deposit of thickness greater than 5 mm was continuously distributed as sand sheets. We followed the definition of *Abe et al*. [2015], but we actually found that storm deposits can be distributed not only continuously, but also intermittently as shown below.

To consider the influence of vegetation during the sediment transport calculation, Delft-3D's trachytope module [*Deltares*, 2011] was used. By using this module, higher bed shear stress and larger sediment transport rates due to the presence of vegetation (which would occur if the same vegetation-enhanced bottom roughness was applied to both hydrodynamics and sediment transport) can be avoided [*Holland et al*., 2010], so that the effect of vegetation on inhibiting sediment transport is reproduced. In this module, a $-\frac{\lambda}{2}u^2$ term is included in the momentum equation. Therein, λ is the flow resistance of the vegetation and u is velocity. For the case of nonsubmerged vegetation ($h < h_v$), the flow resistance and bed roughness are described as below.

$$C = C_b \tag{1}$$

$$\lambda = C_D n \tag{2}$$

C is the Chezy roughness, λ is the flow resistance of the vegetation. C_b is the alluvial bed roughness, C_D is the drag coefficient, n is the vegetation density, h_v is the vegetation height, and h is the water depth. In the case of submerged vegetation ($h > h_v$), the equations are as below.

$$C = C_b + \frac{\sqrt{g}}{\kappa}\ln\left(\frac{h}{h_v}\right)\sqrt{1+\frac{c_D n h_v c_b^2}{2g}} \tag{3}$$

$$\lambda = C_D n \frac{h_v c_b^2}{h c^2} \tag{4}$$

Therein, κ is the Von Kaŕmaǹ constant and g is the gravitational acceleration. Near Tacloban, the beach is bare, and vegetation mainly grows landward of the sand dune, based on field studies and the inspection of

Table 1. Studied Cases and Assumptions

Cases	Vegetation	Vegetation Type	Grain Size	Waves	Typhoon
Case 1	Y	Grass mixture	Fine	Y	Actual
Case 2	Y	Grass mixture	Medium	Y	Actual
Case 3	Y	Grass mixture	Coarse	Y	Actual
Case 4	N		Fine	Y	Actual
Case 5	Y	Grass mixture	Fine	N	Actual
Case 6	Y	Grass mixture	Fine	Y	Strong
Case 7	Y	Grass mixture	Fine	Y	Weak
Case 8	Y	Grass mixture	Fine	Y	Fixed at Tacloban
Case 9	Y	Production grassland	Fine	Y	Actual
Case 10	Y	Cattail	Fine	Y	Actual

satellite images. Therefore, in domain D3, we specified the area landward of the sand dune as being vegetated.

3.2. Parameter Study

An advantage of numerical simulation is the capability to assess what parameters control the formation of storm deposits. We therefore conducted calculations varying the following five parameters and compared to Case 1 (Table 1), which was assumed to be closest to reality.

1. Grain size (Cases 1, 2, and 3): Because settling velocity varies depending on grain size, the maximum inland extent of sand deposition may also be affected by this parameter. The storm deposits located at the inland extent of deposition in Tacloban was mainly composed of very fine sand, but the distribution varied both vertically and horizontally. Therefore, in order to consider the effect of grain size, calculations were run with very fine sand (0.1 mm: Case 1), medium sand (0.3 mm: Case 2), and very coarse sand (2.0 mm: Case 3) as well.
2. Bottom roughness (Case 4): Bottom roughness (the presence of vegetation) may greatly affect the result of the sediment transport calculation. To examine its effect, we additionally ran a calculation without vegetation (Case 4).
3. Waves (Case 5): During a typhoon, water level rises (storm surge) due to low pressure and strong winds, while storm waves are incident from offshore. In order to examine whether storm surge or waves contribute to the formation of sand deposits, storm surge alone was considered (Case 5), without waves present. In Case 5, the water level setup due to barometric pressure and wind-induced storm surge was calculated by Delft-3-D, but SWAN was not implemented.
4. Intensity of typhoons (Cases 6 and 7): The inland distribution distance of the sand layer is defined as the distance from the shoreline to which a sand thickness of more than 5 mm was continuously distributed as sand sheets. This may be affected by typhoon intensity because the size of waves and storm surge is a function of intensity of the typhoon. Thus, we conducted simulations with increased typhoon intensity (Case 6: category 5 typhoon with 140 kt maximum wind speed and 870 hPa central pressure) and decreased intensity (Case 7: category 3 typhoon with 100 kt maximum wind speed and 960 hPa central pressure).
5. Duration of wave incidence (Case 8): The thickness of storm deposits may be affected by the duration of wave incidence. Therefore, we examined whether sand thickness and deposit formation time are affected by assuming that the typhoon was fixed in place until the end of the calculation at its location at 8:00 A.M. on 8 November (the time at which wind speed in Tacloban was the highest) (Case 8).
6. Vegetation types (Cases 9 and 10): Both inland inundation limit and maximum inland extent of sand may be affected by vegetation type. Therefore, other types of vegetation were examined. In Case 9, production grassland was assumed. Based on *Baptist* [2005], its vegetation height (m), stem diameter (m), and number of stems per square meter (stems/m^2) are set as 0.06, 0.003, and 15000, respectively. In Case 10, cattail was assumed. Based on *Baptist* [2005], its vegetation height, stem diameter, and number of stems are 1.5, 0.0175, and 20, respectively.

4. Results

4.1. Validity of the Numerical Results (Case 1)

The maximum significant wave height in the first domain was about 19 m (Figure 2), which is consistent with the results of *Bricker et al.* [2014]. The numerical result was then verified by comparing the measured

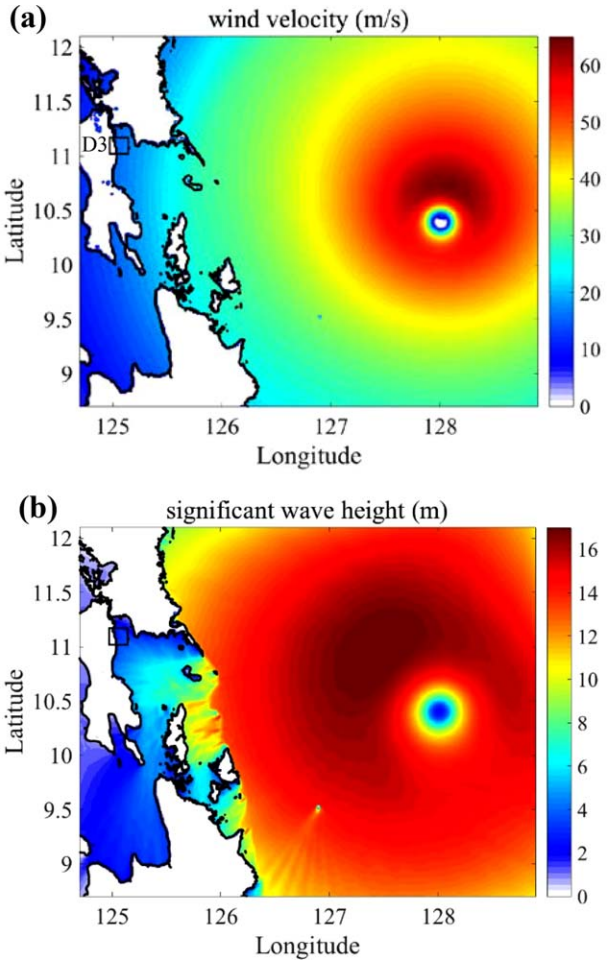

Figure 2. (a) Wind field (m/s) of Typhoon Haiyan on 7 November, 11:00 P.M. in the first domain [after *Bricker et al.*, 2014]. (b) The distribution of significant wave height (m) in the first domain estimated by the wind field on 7 November, 11:00 P.M.

[*Tajima et al.*, 2014; *Mori et al.*, 2014] and computed flow depths at 28 points in Tacloban using K and κ parameters [*Aida*, 1978]. Therein, K and κ indicate geometric average value, and a measure of fluctuation in the ratio of observed to computed amplitudes, respectively. In our case, $K = 1.22$ and $\kappa = 1.28$ (Figure 3). *Takeuchi et al.* [2005] suggested that $0.8 \leqq K \leqq 1.2$ and $\kappa \leqq 1.6$ are required to accurately reproduce the measured values. Our results showed that κ was within this range but K was slightly overestimated, indicating that observed flow depths are larger than computed depths. Calculated flow depths were less than the measured values at the sites where large flow depths (>6 m) were recorded (Figure 3). These sites were located close to the shoreline, and the effects of local undulations such as the presence of sand dunes may have had a significant effect here. However, because of the mesh size in our model, such local undulations were not reproduced well. This may be one reason why calculated flow depths around the shoreline were underestimated. Alternatively, local effects such as wave splash, which could not be reproduced by numerical modeling, might have affected the field measurements. Furthermore, it is possible that the assumption of constant roughness used in the area near the shoreline, and the exclusion of phase-resolving gravity and infragravity wave motions from the model, may cause this discrepancy.

For the same reasons, calculated flow depths are less than measured values within 100 m of the shoreline along the Tolosa and Tanauan transects (Figure 4). On the other hand, the calculated flow depth 800 m inland along the Tanauan transect was too deep (Figure 4a). This is probably because the flow depth 800 m inland in Tanauan was measured behind a structure [*Abe et al.*, 2015]. Therefore, wave incidence might have been prevented by the structure and thus the water depth at this site might have been low. However, this effect was not reproduced in the calculation.

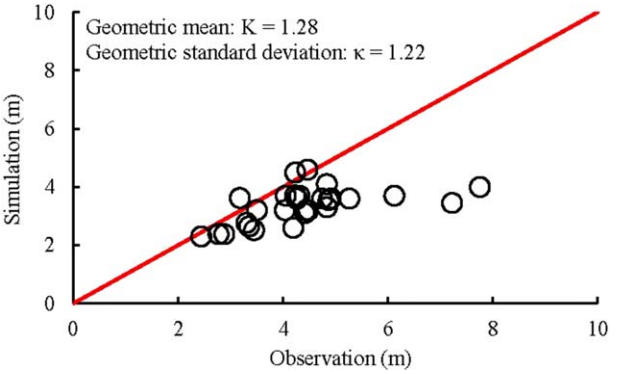

Figure 3. Measured [*Mori et al.*, 2014] and calculated flow depths (m) at Tacloban.

Calculated inundation limits were consistent with measured ones: measured and calculated inundation limits were 3100 and 2800 m, respectively, along the Tanauan transect, and 1400 and 1200 m along Tolosa transect (Figure 4).

We then verified the reproducibility of the sediment transport calculation. Numerical results indicate that sandy deposits continuously extended as sand sheets up to

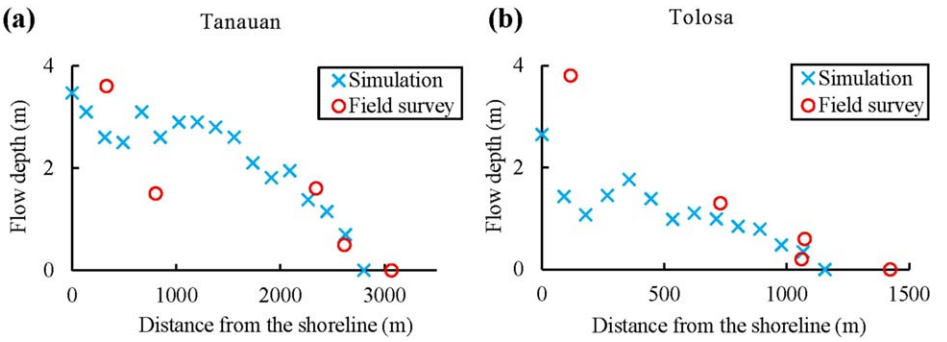

Figure 4. Measured (red point) [*Mori et al.*, 2014] and calculated (blue point) flow depths (m) on (a) Tanauan and (b) Tolosa transects. Note that calculated inundation limits are consistent with the field survey results.

223 m from the coast along the Tanauan transect (Figure 5) and 89 m along the Tolosa transect (Figure 6). These are consistent with the values measured by *Abe et al.* [2015]. On the other hand, discontinuous sand deposits further extended up to 670 m inland. This is because thin deposits (with a thickness on the order of millimeters) were locally formed in a low-lying depression (Figure 5c). Although the extent of continuous sand sheets should be adopted as the criterion for determining the inland deposition limit in order to

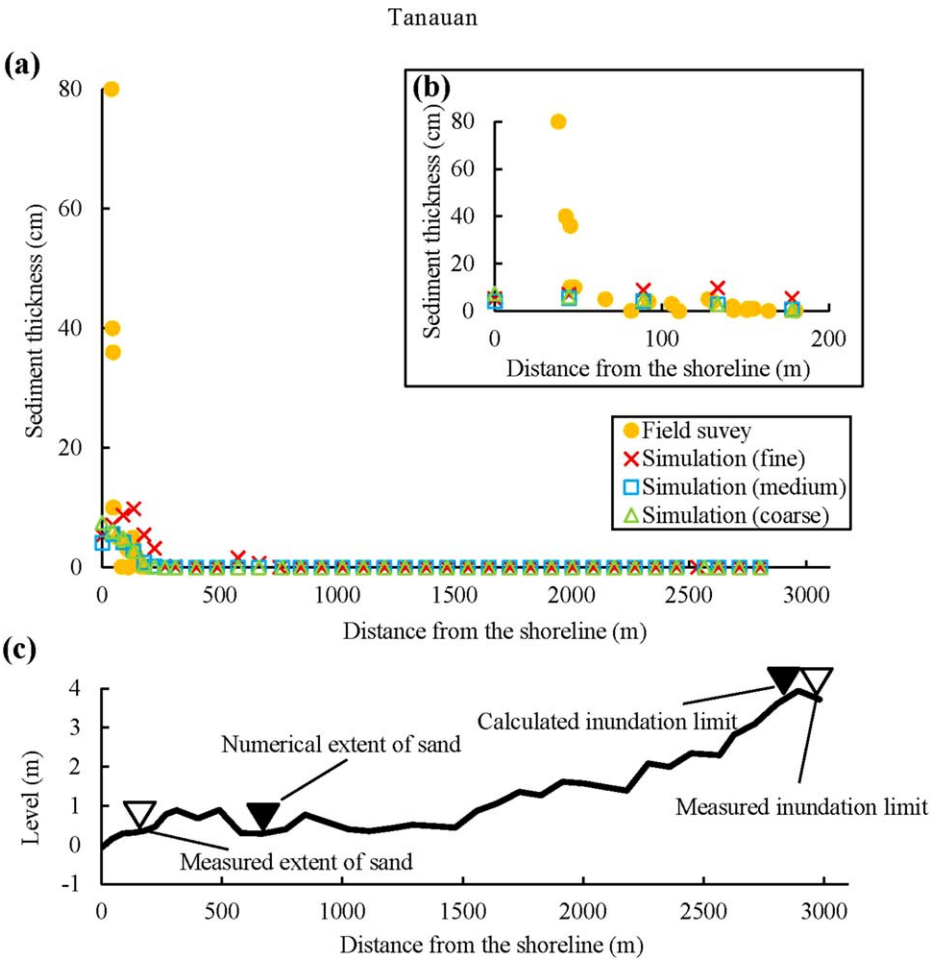

Figure 5. (a) Comparison between the measured and calculated thickness of the sand layer along the Tanauan transect. (b) Close up figure from the shoreline to 200 m inland along the Tanauan transect. Red point: very fine sand (0.1 mm, Case 1), blue point: medium sand (0.3 mm, Case 2), green point: very coarse sand (2.0 mm, Case 3). (c) A cross-sectional profile along the Tanauan transect used in our simulation. Maximum extent of sand derived by field survey [*Abe et al.*, 2015] and our simulation is also shown.

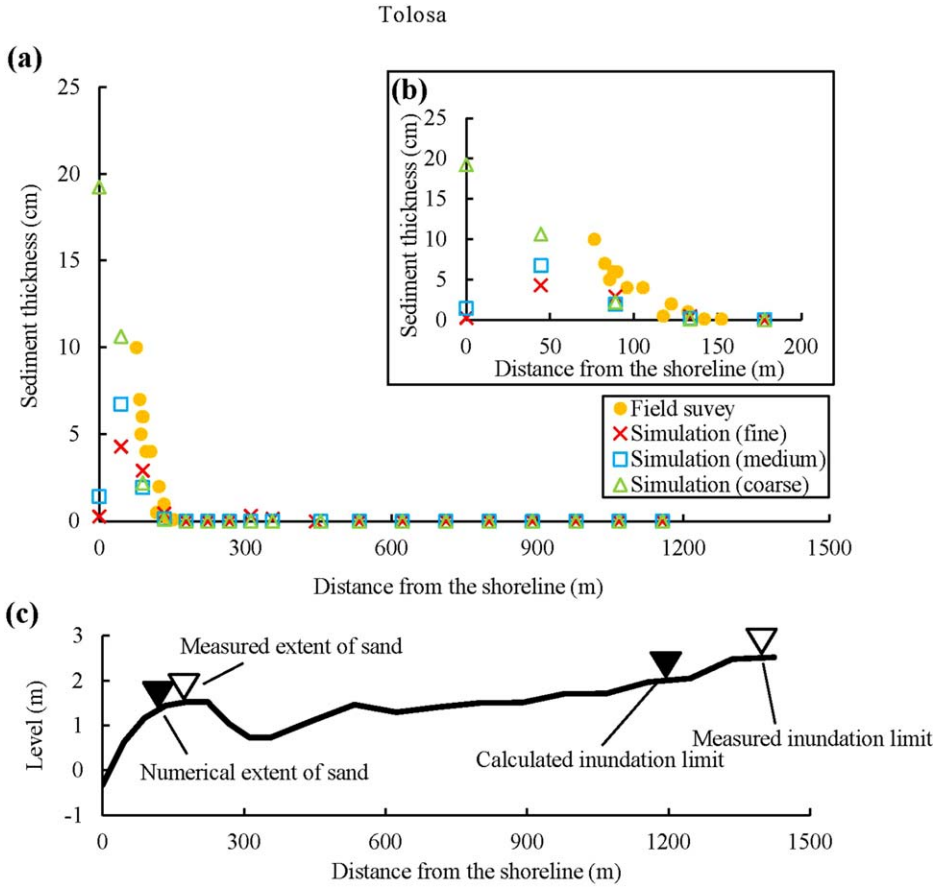

Figure 6. (a) Comparison between the measured and calculated thickness of the sand layer along the Tolosa transect. (b) Close up figure from the shoreline to 200 m inland along the Tolosa transect. Red point: very fine sand (0.1 mm, Case 1), blue point: medium sand (0.3 mm, Case 2), green point: very coarse sand (2.0 mm, Case 3). (c) A cross sectional profile along the Tolosa transect used in our simulation. Maximum extent of sand derived by field survey [*Abe et al.*, 2015] and our simulation is also shown.

compare with field data as discussed below, the maximum extent of sand including discontinuous sand deposits should be considered in a parameter study. Therefore, hereinafter, we define the distribution limit of the storm deposit as the extent of the discontinuous sand layer of thickness greater than 5 mm.

Calculated sand thickness is generally consistent with measured values in Tanauan (Figure 5) and in Tolosa (Figure 6). However, the calculated sand thickness was underestimated at one point, 50 m inland from the shoreline along the Tanauan transect. This site is located just behind a sand dune, and a maximum sand thickness of 80 cm was measured [*Abe et al.*, 2015]. In our modeling, the mesh size in domain D3 (about 40 m) was not able to resolve the sand dune well and thus not only the inundation but also the source of the sandy deposit were not fully reproduced. Therefore, both bed shear stress and sand supply may have been underestimated, resulting in thinner deposits near the shoreline in the calculation.

In summary, we conclude that our numerical results have enough accuracy to examine the overall features of the storm waves and surge as well as sedimentation and erosion along the Tanauan and Tolosa transects. However, local effects, especially near the shoreline, caused some underestimation of the actual inundation and sedimentation.

4.2. Estimated Inundation and Sedimentation Processes (Case 1)

Numerical results showed that the typhoon approached close to Tacloban on 8 November at 7:00 A.M. Philippine time. Then, inundation started and the maximum water level of 5.0 m was recorded at Tacloban at 9:45 A.M. When the typhoon moved away from Tacloban, the waves dissipated, and the water level gradually subsided. The water inundated further inland north of 11.1°N than south of this latitude (Figure 7a). This is because the land elevation to the south is as high as about 3 m, while it is only about 1 m elevation to

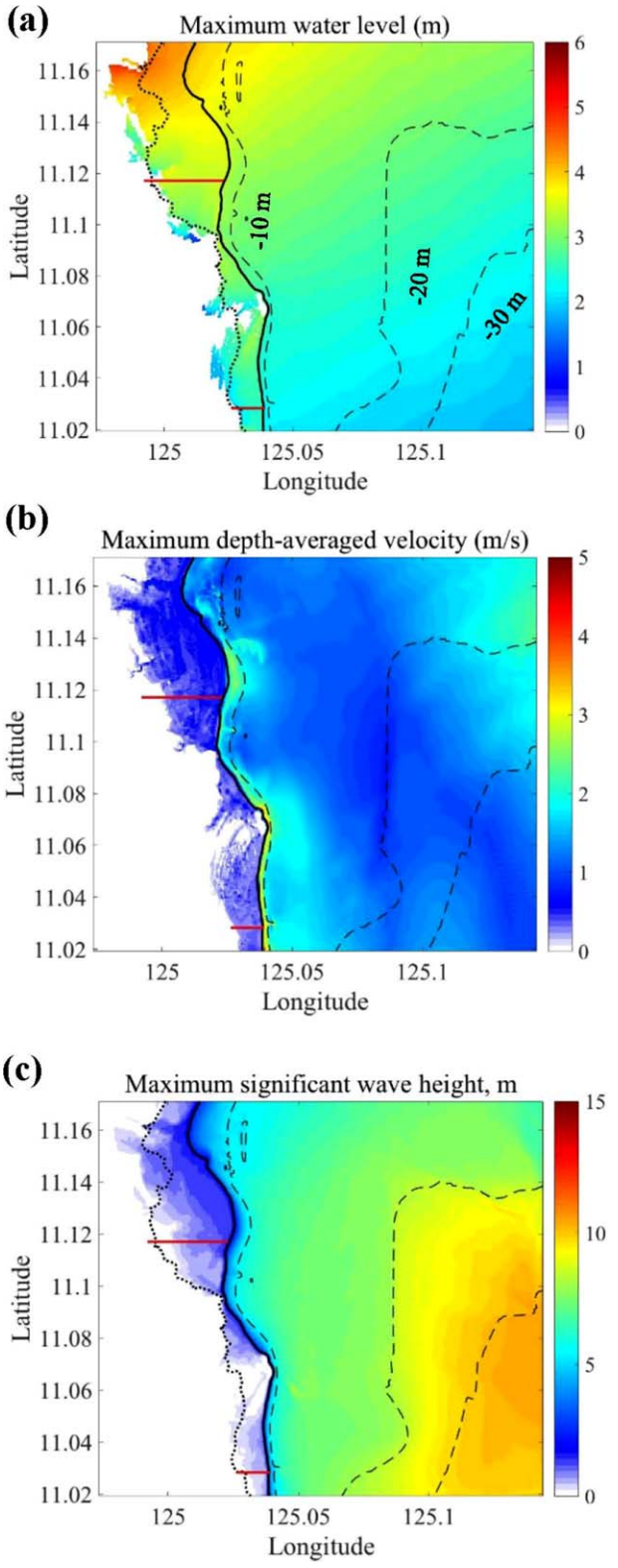

Figure 7. Distributions of (a) maximum water level (m) from mean sea level (dashed line is inundation limit estimated by *Yi et al.*, [2015]), (b) maximum flow speed (m/s), and (c) maximum significant wave height (m) in the third domain. Offshore dotted line shows depth contours at 10 m intervals. Approximate locations of Tanauan and Tolosa transect are also shown as red lines.

the north. The significant wave height and mean flow velocity near the mean sea level shoreline in domain D3 were about 8 m and 2.0 m/s, respectively (Figures 7b and 8c). However, neither strong flow speeds nor waves were seen further inland than 100 m from the normal shoreline.

The flux of suspended and bed load transport in domain D3 was maximum between the shoreline and the 10 m water depth contour (Figure 8). The maximum erosion and sedimentation in this zone were 410 cm and 129 cm, respectively (Figure 9a). In Figure 10, time series of the sand layer thickness, mean current velocity generated by wave setup and storm surge, orbital velocity generated by waves, and the maximum bed shear stress induced by storm surge and waves were calculated 89 m inland from the shoreline along the Tolosa transect (6 cm storm deposit thickness) and 92 m inland from the shoreline along the Tanauan transect (4 cm storm deposit thickness). Hereinafter, we call these points as reference points in order to compare with other cases in section 4.3. The typhoon passed from south to north so that inundation and sedimentation started in Tolosa earlier than in Tanauan. The maximum bed shear stress near the shoreline was recorded at about 8:00 A.M. in both transects, and sedimentation began after that (Figure 10). Around 2:00 P.M. after the typhoon had departed, the maximum bed shear stress became significantly weaker, and sedimentation and erosion on land ceased. Our result indicates that sandy storm deposits formed over the course of these 7 h.

4.3. Parameter Study

4.3.1. Effect of Grain Size (Cases 2 and 3)

Offshore erosion and sedimentation increased with decreasing grain size (Figure 9). Maximum inland extent of sand along the Tanauan transect increased when the calculation was conducted by using finer sand rather than coarser sand (Table 2), because sediment can be moved easier if grain size is smaller. However, along the Tolosa transect, maximum inland extent of sand did not vary with grain size (Table 2). This difference between the Tol-

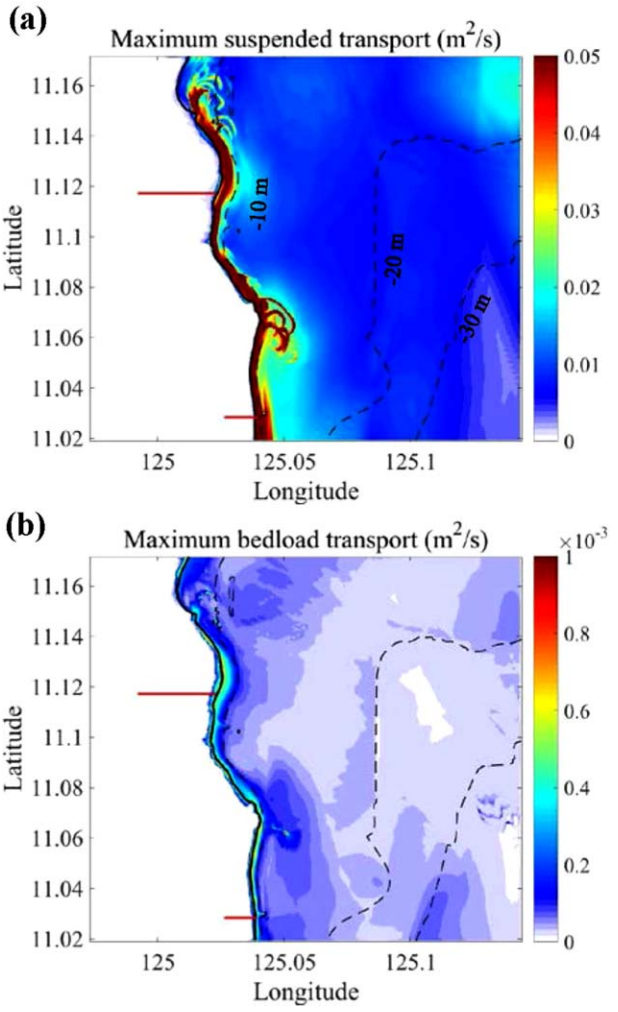

Figure 8. Maximum fluxes of (a) suspended transport and (b) bed load transport near Tacloban. Bed load and suspended load transport were greatest near the shoreline. Offshore-dotted line shows depth contours at 10 m intervals. Approximate locations of Tanauan and Tolosa transect are also shown as red lines.

osa and Tanauan transects is the height of the dune near the shoreline, which is higher (~1.5 m) in Tolosa than in Tanauan (Figure 6).

4.3.2. Effect of Vegetation (Case 4)

For the no-vegetation case, the roughness coefficient on land was small, and hence sediments were transported far inland. Moreover, in this case, the propagation distance of waves inland along the Tanauan transect was the largest (Figure 11) so that the duration time of waves acting on sediments is long. Along the Tolosa transect, the propagation distance inland of waves increased compared to Case 1. Consequently, sediments were transported further inland compared to other cases. In fact, sandy deposits formed up to 1500 m inland along the Tanauan transect and 310 m inland along the Tolosa transect. These distances are far longer than those in Case 1 (Figure 12), suggesting that vegetation greatly affects the maximum inland extent of sand deposition.

4.3.3. Effect of Storm Waves (Case 5)

For the no-waves case, total sedimentation, and erosion volumes in domain D3 were small compared to Case 1. Namely, the maximum erosion and sedimentation near the shoreline were 72 and 34 cm, respectively (Figure 13b). This is because the maximum bed shear stress was calculated solely from the mean current velocity due to storm surge in Case 5, whereas it was calculated due to both storm surge and waves in Case 1. This in turn implies that storm waves are critically important for suspension of sediments.

4.3.4. Effect of Typhoon Intensity (Cases 6 and 7)

The maximum extent of sand increased on both transects in Case 6 as compared to Case 7. This is because wave height and the inland extent of wave propagation along both transects were larger in Case 6 compared to Case 7, so that the wave-induced shear stress on land was also larger in Case 6. In contrast, both inundation distance and maximum extent of sand were smaller in Case 7. Details are shown in Tables 2 and 3.

4.3.5. Effect of Wave Duration (Case 8)

In Case 8, waves were continuously strong until the end of simulation (12:00 P.M.). Therefore, the maximum bed shear stress did not weaken (Figure 10), and sedimentation continued. Consequently, sand thicknesses at the reference points cumulatively increased to 86 cm on the Tanauan transect and 5.6 cm on the Tolosa transect (Figure 10). In Case 8, initiation of sedimentation was delayed compared to Case 1. This is because the track of the typhoon was different in these cases.

4.3.6 Vegetation Types (Cases 9 and 10)

In Case 9, inundation limits along both transects increased compared to Case 1 (Table 2). This is because the vegetation height was larger in Case 9, even though the stem density was smaller. The maximum inland extent of sand also increased along both transects (Table 2) in Case 9 compared to Case 1 because vegetation height was smaller, so that bed shear stress acting on sediments decreased.

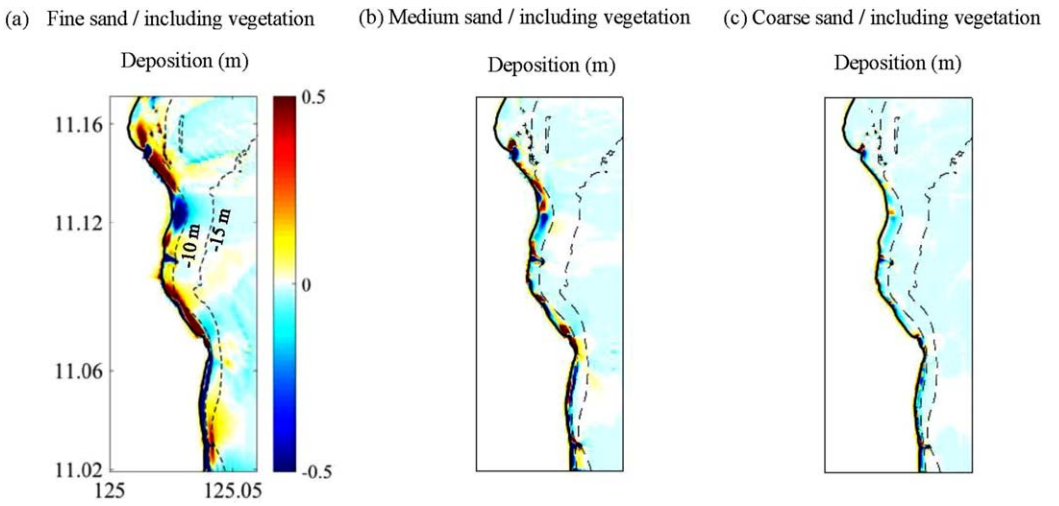

Figure 9. The results of sediment transport calculation near the shoreline in case that grain size was changed to (a) very fine sand (Case 1), (b) medium sand (Case 2), and (c) very coarse sand (Case 3). Positive and negative values indicate sedimentation and erosion, respectively.

In Case 10, the inundation limit along the Tanauan transect decreased, and maximum extent of sand also decreased compared to Case 1 (Table 2). In this case, vegetation height and stem diameter were larger, and vegetation density was smaller compared to Case 1. Due to the increase of vegetation height and stem diameter, inundation limit and maximum inland extent of sand became shorter.

In summary, vegetation height and stem diameter are important for determining the inundation limit and sand distribution.

5. Discussion

In this section, we first discuss the reason why the maximum inland extent of storm deposits is small compared to the inundation distance. Then, we discuss the main factors affecting the distribution of sandy storm deposits. Finally, implications to the identification of tsunami and storm deposits are discussed.

5.1. Why the Sediment Was Not Transported Far Inland

As described in section 4.1, large shear stresses were not generated on land because waves were significantly dissipated before propagating inland (Figure 7c). Moreover, as described in section 4.3.3, sedimentation and erosion are generated by storm waves more than by storm surge. Therefore, sediments were not transported far inland, but were deposited near the shoreline. Consequently, the maximum inland extent of storm deposits was significantly shorter than the inundation limit.

It should be noted that the above mentioned sedimentary process may not be applicable if longer waves were generated. For example, surf-beat was generated during the 2013 typhoon in Hernani in Eastern Samar [*Roeber and Bricker*, 2015]. Therein, the inundation distance from the shoreline along the coast of Eastern Samar was 800 m [*Tajima et al*., 2014; *Shimozono et al*., 2015; *May et al*., 2015]. Numerical simulation of surf-beat showed that the frequency was 0.0035 Hz, which is equivalent to a period of 286 s [*Roeber and Bricker*, 2015]. Under such circumstances, the deposition ratio might have been higher, and extended further inland, than that at Tacloban, although no geological survey at this site has been conducted so far.

It is important to note that local topography may greatly affect the maximum extent of sand deposits. In fact, *Pilarczyk et al*. [2016] reported that sandy storm deposits in Leyte Gulf formed by Typhoon Haiyan were distributed up to 1.7 km inland from the shoreline, while the inundation limit was 2.0 km. Therefore, maximum extent of sand may not be constrained only by the inundation distance, but local topography, which affects the local inundation pattern, should also be considered to assess the sediment transport process. In this sense, numerical modeling would be a strong tool to use in exploring the relationship between the inundation limit of storm surge and the maximum inland extent of sand deposits.

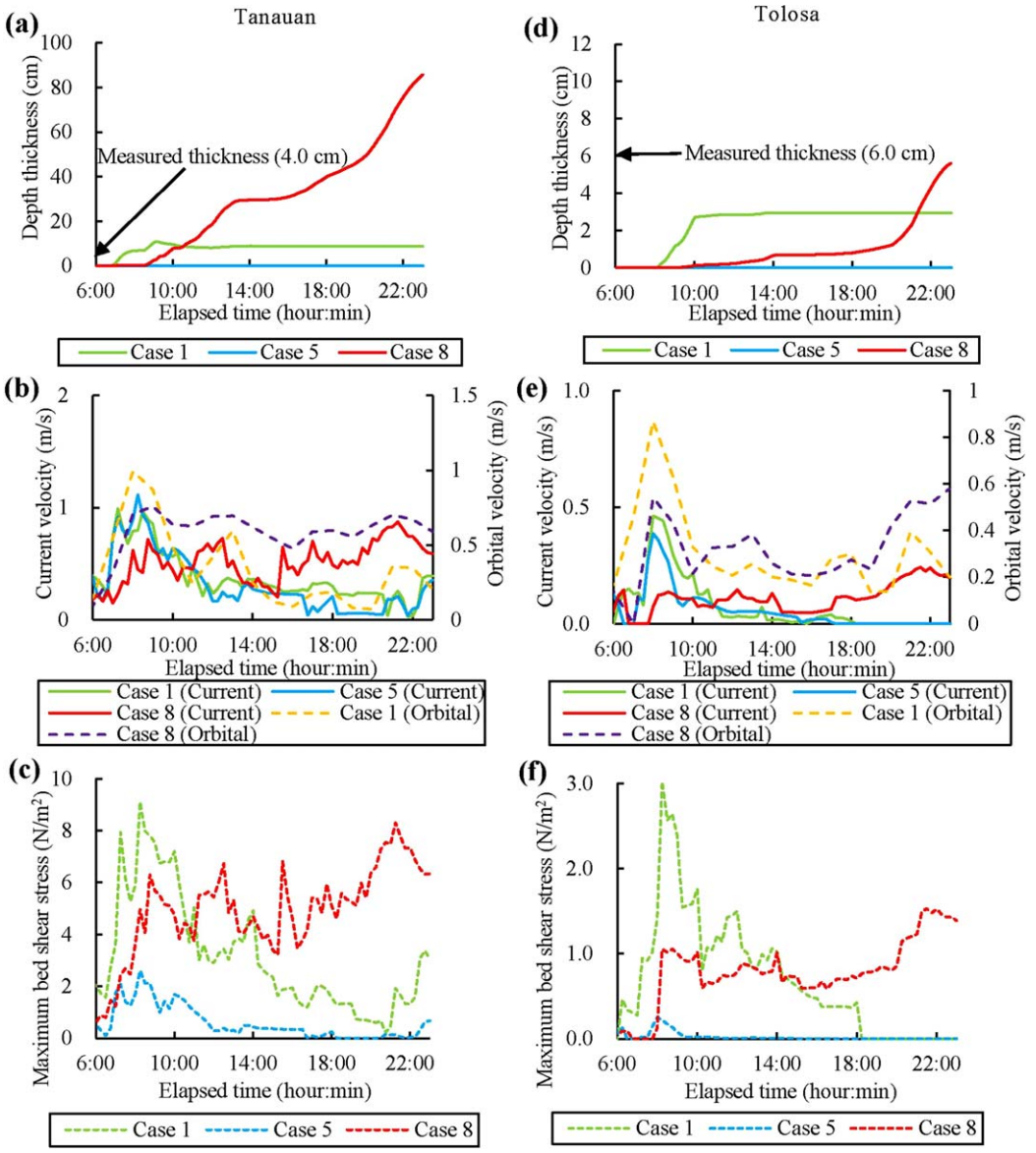

Figure 10. Time series variations of (a) the thickness of the deposit, (b) the mean current velocity and orbital velocity, and (c) maximum bed shear stress at 92 m inland from the shoreline along the Tanauan transect. Time series variations of (d) the thickness of the deposit, (e) mean current velocity and orbital velocity, and (f) maximum bed shear stress at 89 m inland from the shoreline along the Tolosa transect in Cases 1, 5, and 8. Note that mean current velocity is generated by wave setup and storm surge while orbital velocity is generated by waves. The maximum bed shear stress is generated by both storm surge and waves.

Table 2. Inundation Distance (m) and Maximum Inland Extent of Sand (m) in All Cases

Cases	Inundation Distance in Tanauan (km)	Inundation Distance in Tolosa (km)	Maximum Extent of Sand in Tanauan (km)	Maximum Extent of Sand in Tolosa (km)
Case 1	2.8	1.2	0.67	0.089
Case 2	2.8	1.2	0.18	0.089
Case 3	2.8	1.2	0.13	0.089
Case 4	4.1	1.3	1.5	0.31
Case 5				
Case 6	3.6	1.3	0.80	0.36
Case 7	1.7	0.40	0.58	0.045
Case 8				
Case 9	3.5	1.3	0.98	0.36
Case 10	2.6	1.2	0.58	0.089

As stated above, calculated maximum inland extents of continuous sand sheets are well consistent with the measured values along both transects. However, along the Tanauan transect, we found that deposits were intermittently observed far beyond the inland limit of continuous sand sheets. This is probably related to the local topography. In

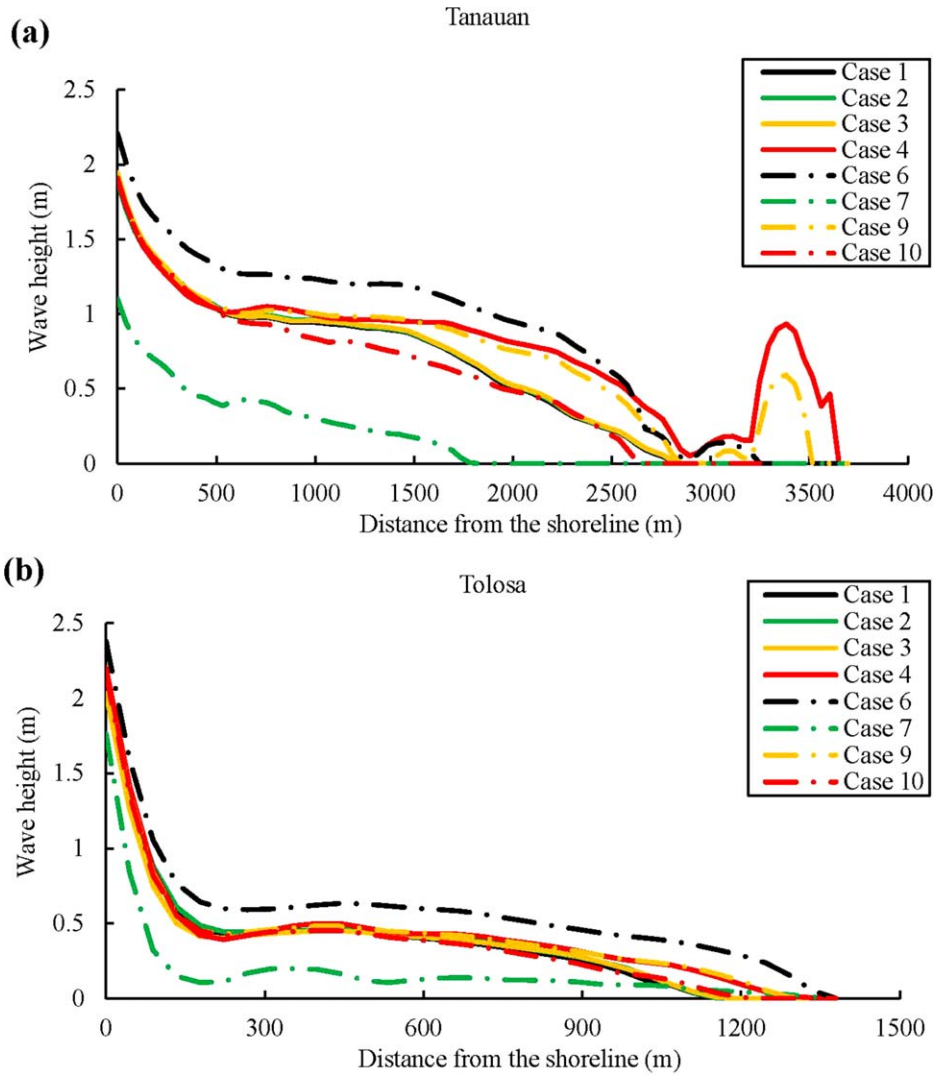

Figure 11. The calculated wave height along (a) Tanauan and (b) Tolosa transects in each case. The results in Cases 5 and 8 are not shown because wave height was not calculated in these cases.

fact, no sediments were observed on (inland-facing) downward slopes, while thin deposits formed in a low-lying depression (Figure 5c). This result infers that, when delineating the inland limit of sand deposits, such local, irregular deposits are important to consider, although such local and minor sedimentation may be difficult to recognize during a field survey.

5.2. Parameters That Characterize the Sand Layer Thickness and Distribution of Storm Wave Deposits

It is obvious from Figure 10 that scale and duration of bed shear stress control the resultant sand layer thickness. Bed sear stress is controlled by the orbital velocity, which is generated by waves. Thus, we infer that the orbital velocity induced by waves is the dominant factor in determination of the resultant sand layer thickness.

Moreover, water depth greatly affects the sand distribution. Figure 12b shows that there is a good correlation between maximum inland extent of sand and maximum water depth, because the maximum inland extent of sand increases with increasing maximum water depth. Therefore, variation of water depth and its error will greatly affect sand deposition since water depth controls the distribution of wave height and consequent sedimentation.

From Table 3, it is obvious that deposition ratio increases with decreasing roughness coefficient or increasing typhoon intensity, suggesting that these parameters are major factors in determining the maximum

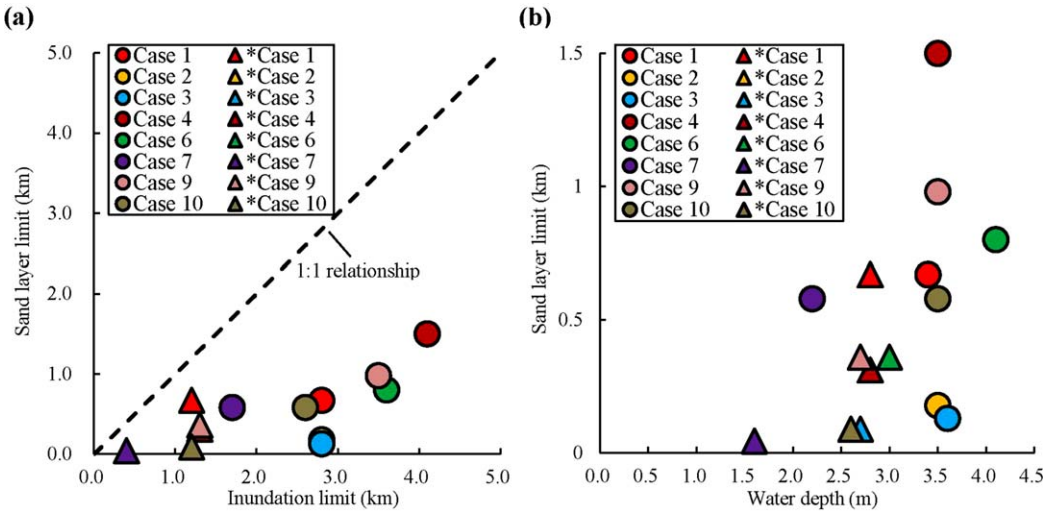

Figure 12. Diagrams showing (a) inundation limit versus maximum extent of sand, and (b) maximum water depth on both transects versus maximum extent of sand. Case∼: results along Tanauan transect, *Case∼: results along Tolosa transect. For Cases 5 and 8, the maximum extent of sand was not examined because these cases are physically unrealistic and used only for the model sensitivity analysis.

extent of storm deposits. However, in Case 7, deposition ratio was the highest of all cases. This is because, although the maximum extent of sand was smaller than in other cases, the inundation distance was also small.

Given these issues, can we estimate the inundation distance of past storm events from the measured maximum inland extent of storm deposits? The deposition ratio is 0.37 in the case without vegetation (Table 3, Case 4). Even though this is the maximum value among the realistic study cases, it is still very small. Therefore, the maximum inland extent of storm deposits alone may not be a straightforward factor to use in estimating the inundation distance. Instead, forward or inverse (or hybrid) modeling is required to better estimate the inundation distance from storm deposits. During the numerical modeling process, reproduction of the appropriate distributions of vegetation during historical events would be the key to accurately estimating the inundation limits from the measured distributions of storm deposits during these events. This is because inundation limit and sand distribution vary significantly with assumed values of vegetation height and stem diameter (Table 2).

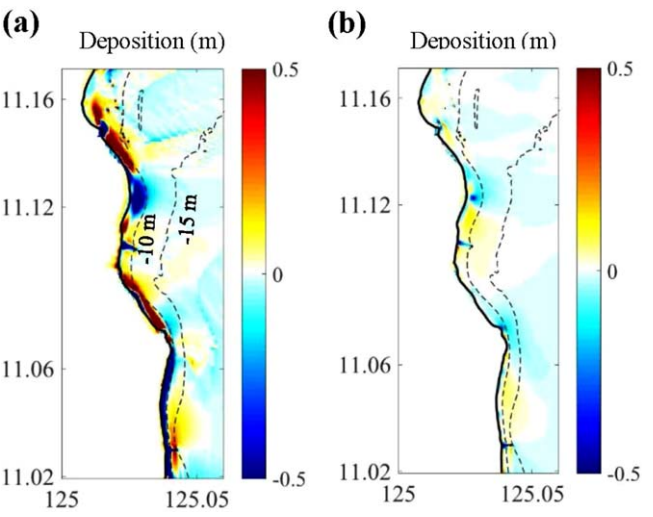

Figure 13. The results of sediment transport calculation for the cases where (a) waves were included in simulation (Case 1) and (b) waves were not included (Case 5). Positive and negative values indicate sedimentation and erosion, respectively.

5.3. Implication on the Identification of Deposits Formed by Extreme Waves

As previously reported [e.g., *Morton et al.*, 2007; *Phantuwongraj et al.*, 2013], our results show that the maximum inland extent of storm deposits is small compared to inundation distance. A parameter sensitivity analysis further revealed that the presence or absence of vegetation on land, as well as the intensity of the typhoon, significantly affect the maximum inland extent of sand deposits, because the distribution of vegetation and intensity of the typhoon are critical to the determination of the bed shear stress acting on sediments. As local sedimentation occurred inland far beyond the limit of continuous sand sheets, it can be seen

Table 3. Deposition Ratio and Maximum Sediment Thickness (cm) in All Cases

Cases	Deposition Ratio in Tolosa	Deposition Ratio in Tanauan	Maximum Sediment Thickness in Tanauan (cm)	Maximum Sediment Thickness in Tolosa (cm)
Case 1	0.077	0.24	9.8	4.3
Case 2	0.077	0.064	5.5	6.7
Case 3	0.077	0.046	6.1	11
Case 4	0.24	0.37	12	7.5
Case 5				
Case 6	0.28	0.22	15	8.5
Case 7	0.11	0.33	5.9	1.0
Case 8			86	5.6
Case 9	0.28	0.28	17	4.1
Case 10	0.074	0.22	9.1	5.5

that grain size and local topography also affect the maximum inland extent of sand deposits.

Similar to the Haiyan case, *Morton et al.* [2007] reported that the maximum extent of sandy deposits formed by the 2003 Hurricane Isabel was 930 m inland from the shoreline, while its inundation limit was 15–30 km. They also reported that the maximum extent of sandy deposits during the 1961 Hurricane Carla was 260 m while its inundation limit was 15–35 km. In these cases, inundation limits were extremely large but could greatly depend on elevation, slope angle, and distributions of roughness due to vegetation [*Morton et al.*, 2007]. Results by *Phantuwongraj et al.* [2013] also suggests that the deposition ratio was low (=0.33) during typhoons affecting the coast of Thailand between 2007 and 2011. These previous studies as well as our results imply that the maximum extents of sandy storm deposits are typically smaller than inundation limits, although these results may differ [*Pilarczyk et al.*, 2016] with inland topography conditions.

The maximum extent of storm deposits is much smaller than that of tsunami deposits formed by the 2004 Indian Ocean tsunami [e.g., *Jaffe et al.*, 2006] and the 2011 Tohoku-oki tsunami [e.g., *Abe et al.*, 2012]. In case of tsunami deposits, it is reported that sandy deposits formed by the 2011 Tohoku-oki tsunami on the Sendai plain were distributed inland up to 57–76% of the inundation distance [*Goto et al.*, 2011; *Abe et al.*, 2012]. *Sugawara et al.* [2014] suggested that sediment transport directed inland by the tsunami was inhibited by artificial structures such as dikes. Moreover, although sufficient tsunami flow speeds necessary to erode sediments on land were generated, sediment sources did not exist on land so that onshore resuspension did not occur [*Sugawara et al.*, 2014].

Cheng and Weiss [2013] revealed that the main factors in determining maximum inland extent of sand deposited by tsunamis are wave amplitude and onshore slope, while grain size does not greatly affect the inland distribution limit. However, our results revealed that grain size is critical in determining maximum inland extent of sand during storms because intermittent deposits locally formed at inland sites where elevations are low, beyond the limit of continuous distribution of sand sheets.

A main difference between tsunami and storm surge/waves is flow speed on land. In case of the 2011 Tohoku-oki tsunami, flow speed was fast (>3 m/s at a location several kilometers inland from the shoreline) so that sediments could have been transported far inland [*Sugawara et al.*, 2014]. Due to the difference in hydraulic processes between storm surge/waves and tsunamis, the maximum inland extent of storm deposits compared to the storm's inundation limit will generally be smaller than those of tsunami deposits in a similar topographic setting. This in turn implies that tsunami deposits can be differentiated from storm deposits if we consider the difference of their maximum inland extents. For example, it is possible to calculate the maximum inland extent of sandy storm deposits by assuming the maximum possible typhoon, which may be estimated by measurements, meteorology, history, and geology. Then, if actual deposits were distributed farther inland than the calculated inland distribution limit of storm deposits, it is likely that those deposits were formed by a tsunami instead. It should be noted, however, that identification through this numerical approach of the origin of deposits distributed near the shoreline may be difficult, because deposits close to the shoreline can be explained by both tsunami and storm surge/waves.

Alternatively, our results imply that the difference in sedimentary structure due to a difference in the time it takes deposits to form may also be useful for the differentiation between storm and tsunami. In case of the 2011 Tohoku-oki tsunami, the first wave was the dominant cause of sedimentation [e.g., *Sugawara et al.*, 2014]. *Sugawara et al.* [2014] calculated that sedimentation ceased about 4 min after the tsunami reached the shoreline. Similarly, *Yamada et al.* [2014] reported that sandy tsunami deposits formed by the 2011

Tohoku-oki tsunami in Miyako city, Iwate Prefecture were deposited within several minutes after the first tsunami wave reached the shoreline. Of course, it is possible that tsunami deposits would continue forming over a long time if subsequent waves are also large. However, even in such a case, it is unlikely that more than just a few waves would cause onshore sedimentation.

In contrast, storm deposits are formed over a long time (a few hours) because of the slow movement of typhoons (Figure 10). During Typhoon Haiyan, several hundreds to thousands of incident waves could have contributed to formation of sand deposits during the time the typhoon was close to the coast (~5–7 h). In hypothetical Case 8, formation of deposits continued for about 15 h as the typhoon was fixed in position near Tacloban. Within this time span, far more waves caused the sedimentation of storm deposits near the shoreline and hence thicker sediment deposits were formed. Considering the great number of waves contributing to storm deposits, it is likely that multiple layers can form within storm deposits near the shoreline. In fact, multiple layers in storm deposits have often been reported [e.g., *Phantuwongraj et al*., 2013]. Therefore, our results imply that the existence of multiple layers can be used as an identification proxy of storm deposits as previously suggested by *Morton et al*. [2007].

Our calculation further revealed that the sand thickness of storm deposits becomes thicker in Case 8 because of the long sedimentation time. Measurements also show that the thickness of storm sand deposits tends to be larger than those of tsunami deposits [e.g., *Morton et al*., 2007]. Therefore, the thickness distribution may be another candidate for differentiating deposits formed by storm versus tsunami. However, local tsunami deposits with large thickness have also been reported [*Peters and Jaffe*, 2010]. Further research is required to compare the difference of thickness distribution between storm and tsunami deposits. Moreover, for better understating of the sedimentation process of sandy deposits, the comparison of bedload and suspended load transport between tsunamis and storms should be investigated in the future.

6. Conclusions

We examined the factors controlling sedimentation due to storm waves and surge based on numerical simulations under various conditions. The study revealed that the main factors controlling the maximum inland extent and thickness of sandy storm deposits are the typhoon intensity (wave height and water depth) and vegetation (bottom roughness) on land. Grain size may potentially affect local sedimentation. This study also conducted a sensitivity analysis for vegetation and revealed that the assumption of vegetation type and distribution largely affects the inundation limit and consequent maximum inland extent of sand. As previous field studies suggested, the inland distribution limit of storm deposits is short, probably because wave breaking occurred near the shoreline, and total bed shear stress decreased rapidly inland from the breaking location. We also revealed that the duration of wave impact on a coast is longer during a storm than during a tsunami, indicating that multiple layers can form in the internal sedimentary structure of storm deposits and storm deposits tend to be thicker than tsunami deposits. Therefore, a small maximum inland extent of deposits, multiple layers within the deposits, and thicker deposits could be useful as proxies to identify sand deposits as originating from storms instead of tsunamis.

Acknowledgments
We thank T. Abe, D. Sugawara, and A. Suppasri for providing data and for their valuable suggestions and comments. We appreciate the high-resolution digital elevation data provided by Japan International Cooperation Agency for this study. A portion of this study was financially supported by the director of the International Research Institute of Disaster Science (IRIDeS), Tohoku University. All data for this paper are properly cited and referred to in the reference list.

References

Abe, T., K. Goto, and D. Sugawara (2012), Relationship between the maximum extent of tsunami sand and the inundation limit of the 2011 Tohoku-oki tsunami on the Sendai Plain, Japan, *Sediment. Geol.*, *282*, 142–150, doi:10.1016/j.sedgeo.2012.05.004.

Abe, T., K. Goto, D. Sugawara, and A. Suppasri (2015), Geological traces of the 2013 Typhoon Haiyan in the Southeast coast of Leyte Island, Second report of IRIDeS Fact-finding mission to Philippines, pp. 169–174, Tohoku Univ. Int. Res. Inst. of Disaster Sci.

Aida, I. (1978), Reliability of tsunami source model derived from fault parameters, *J. Phys. Earth*, *26*, 57–73.

Apotsos, A., G. Gelfenbaum, and B. Jaffe (2011), Process-based modeling of tsunami inundation and sediment transport, *J. Geophys. Res.*, *116*, F01006, doi:10.1029/2010JF001797.

Baptist, M. J. (2005), Modelling floodplain biogeomorphology, PhD diss. Delft Univ. Press, Delft, Netherlands.

Bricker, J. D., H. Takagi, E. Mas, S. Sure, B. Adriano, C. Yi, and V. Roeber (2014), Spatial variation of damage due to storm surge and waves during Typhoon Haiyan in the Philippines, *J. Jpn Soc. Civil Eng. Ser.*, B2 *70*(2), I_231–I_235.

Cheng, W., and R. Weiss (2013), On sediment extent and runup of tsunami waves, *Earth Planet. Sci. Lett.*, *362*, 305–309, doi:10.1016/j.epsl.2012.12.004.

Dawson, A. G., I. D. Foster, S. Shi, D. E. Smith, and D. Long (1991), The identification of coastal sediment sequences, *Sci. Tsunami Hazards*, *9*, 73–82.

Deltares (2011), *User Manual Delft3D-FLOW*, Deltares, Delft, Netherlands.

Dietrich, J. C., M. Zijlema, J. J. Westerink, L. H. Holthuijsen, C. Dawson, R. A. Luettich Jr, R. E. Jensen, J. M. Smith, G. S. Stelling, and G. W. Stone (2011), Modeling hurricane waves and storm surge using integrally-coupled, scalable computations, *Coastal Eng.*, *58*, 45–65, doi:10.1016/j.coastaleng.2010.08.001.

Egashira, K., I. Fukuda, Y. Kishira, and T. Nishimura (1985), Field measurement of the wave deformation on the reef, *Proc. Coastal Eng., Jpn. Soc. Civ. Eng.*, *32*, 90–94.

Fujii, T., and Y. Mitsuda (1986), *Synthesis of a Stochastic Typhoon Model and Simulation of Typhoon Winds*, vol. 29, pp. B-1, 229–239, Annu. Disaster Prev. Res. Inst., Kyoto Univ.

Goff, J., B. G. McFadgen, and C. Chagué-Goff (2004), Sedimentary differences between the 2002 Easter storm and the 15th-century Okoropunga tsunami, southeastern North Island, New Zealand, *Mar. Geol.*, *204*, 235–250, doi:10.1016/S0025-3227(03)00352-9.

Goff, J., C. Chagué-Goff, S. Nichol, B. Jaffe, and D. Dominey-Howes (2012), Progress in palaeotsunami research, *Sediment. Geol.*, *243–244*, 70–88, doi:10.1016/j.sedgeo.2011.11.002.

Goto, K., K. Okada, and F. Imamura (2009), Characteristics and hydrodynamics of boulders transported by storm waves at Kudaka Island, Japan, *Mar. Geol.*, *262*, 14–24, doi:10.1016/j.margeo.2009.03.001.

Goto, K., et al. (2011), New insights of tsunami hazard from the 2011 Tohoku-oki event, *Mar. Geol.*, *290*, 46–50, doi:10.1016/j.margeo.2011.10.004.

Goto, K., K. Hashimoto, D. Sugawara, H. Yanagisawa, and T. Abe (2014), Spatial thickness variability of the 2011 Tohoku-oki tsunami deposits along the coastline of Sendai Bay, *Mar. Geol.*, *358*, 38–48, doi:10.1016/j.margeo.2013.12.015.

Goto, T., K. Satake, T. Sugai, T. Ishibe, T. Harada, and S. Murotani (2015), Historical tsunami and storm deposits during the last five centuries on the Sanriku coast, Japan, *Mar. Geol.*, *367*, 105–117, doi:10.1016/j.margeo.2015.05.009.

Hawkes, A. D., and B. P. Horton (2012), Sedimentary record of storm deposits from Hurricane Ike, Galveston and San Luis Islands, Texas, *Geomorphology*, *171*, 180–189, doi:10.1016/j.geomorph.2012.05.017.

Holland, G. J. (1980), An analytic model of the wind and pressure profiles in hurricanes, *Mon. Weather Rev.*, *108*, 1212–1218. [Available at https://doi.org/10.1175/1520-0493(1980)108 < 1212:AAMOTW>2.0.CO;2.]

Holland, Van. G., B. Verheyen, S. Jacobs, W. Vandenbruwaene, S. Temmerman, P. Meire, P. Peeters, and J. D. Schutter (2010), Simulation of hydrodynamics and transport of fine sediments in vegetated polders with a controlled reduced tide: Pilot project Lippenbroek, in *Proceedings of the 8th International Symposium on Ecohydraulics 2010 (ISE 2010)*, pp. 1775–1782.

IOC, IHO, and BODC (2003), "*Centenary Edition of the GEBCO Digital Atlas*," published on CD-ROM on behalf of the Intergovernmental Oceanographic Commission and the International Hydrographic Organization as part of the General Bathymetric Chart of the Oceans, Brit. Oceanogr. Data Cent., Liverpool.

Jaffe, B. E., et al. (2006), Northwest Sumatra and offshore islands field survey after the December 2004 Indian Ocean Tsunami, *Earthq. Spectra*, *22*(S3), 105–135, doi:10.1193/1.2207724.

Japan International Cooperation Agency (2014), *JICA-Urgent Development Study on the Project on Rehabilitation and Recovery from Typhoon Yolanda*. [Available at http://www.jica.go.jp/information/seminar/2014/ku57pq00001o1r1z-att/20141205_01_h.pdf.]

Japan Meteorological Agency (2013), *Specialized Meteorological Center Tokyo: Typhoon Center, Best Track Data*. [Available at http://www.data.jma.go.jp/fcd/yoho/data/typhoon/T1330.pdf.]

Kain, L. C., C. Gomez, D. E. Hart, P. Wassmer, J. Goff, and C. Starheim (2014), Assessing topographic controls on flow direction in washover deposits using measurements of Magnetic Fabric, *Mar. Geol.*, *350*, 16–26, doi:10.1016/j.margeo.2014.01.010.

Kennedy, A., N. Mori, Y. Zhang, T. Yasuda, S. E. Chen, Y. Tajima, W. Pecor, and K. Toride (2016), Observations and modeling of coastal boulder transport and loading during super typhoon Haiyan, *Coastal Eng. J.*, *58*(1), doi:10.1142/S0578563416400040.

Mas, E., J. Bricker, S. Kure, B. Adriano, C. Yi, A. Suppasri, and S. Koshimura (2015), Field survey report and satellite image interpretation of the 2013 Super Typhoon Haiyan in the Philippines, *Nat. Hazards Earth Syst. Sci.*, *15*, 805–816, doi:10.5194/nhess-15-805-2015.

May, S. M., M. Engel, D. Brill, C. Cuadra, A. M. F. Lagmay, J. Santiago, J. K. Suarez, M. Reyes, and H. Brückner (2015), Block and boulder transport in Eastern Samar (Philippines) during Supertyphoon Haiyan, *Earth Surf. Dyn.*, *3*, 543–558, doi:10.5194/esurf-3-543-2015.

Mori, N., M. Kato, S. Kim, H. Mase, Y. Shibutani, T. Takemi, K. Tsuboki, and T. Yasuda (2014), Local amplification of storm surge by Super Typhoon Haiyan in Leyte Gulf, *Geophys. Res. Lett.*, *41*, 5106–5113, doi:10.1002/2014GL060689.

Morton, R. A., G. Gelfenbaum, and B. E. Jaffe (2007), Physical criteria for distinguishing sandy tsunami and storm deposits using modern examples, *Sediment. Geol.*, *200*, 184–207, doi:10.1016/j.sedgeo.2007.01.003.

Nagai, T., K. Simizu, M. Sasaki, J. H. Lee, M. Kudaka, and K. Nukada (2007), Characteristic of the Observed Tsunami Profiles of the 2006 and 2007 Chishima-Islands-off Earthquakes, *Proc. Coastal Eng. Jpn. Soc. Civ. Eng.*, *54*, 181–185.

NASA (2014), *Shuttle RADAR Topography Mission (SRTM)*. [Available at http://www2.jpl.nasa.gov/srtm/.]

Peters, R., and B. Jaffe (2010), Identification of tsunami deposits in the geologic record: Developing criteria using recent tsunami deposits. *U.S. Geol. Surv. Open File Rep.*, 2010–1239, 39 p. [Available at http://pubs.usgs.gov/of/2010/1239/of2010-1239.pdf.]

Phantuwongraj, S., and M. Choowong (2012), Tsunamis versus storm deposits from Thailand, *Nat. Hazards*, *63*, 31–50, doi:10.1007/s11069-011-9717-8.

Phantuwongraj, S., M. Choowong, F. Nanayama, K. Hisada, P. Charusiri, V. Chutakositkanon, S. Pailoplee, and A. Chabangbon (2013), Coastal geomorphic conditions and styles of storm surge washover deposits from Southern Thailand, *Geomorphology*, *192*, 43–58, doi:10.1016/j.geomorph.2013.03.016.

Pilarczyk, J. E., B. P. Horton, J. L. A. Soria, A. D. Switzer, F. Siringan, H. M. Fritz, N. S. Khan, S. Ildefonso, and A. A. Doctor, and M. L. Garcia (2016), Micropaleontology of the 2013 Typhoon Haiyan overwash sediments from the Leyte Gulf, Philippines, *Sediment. Geol.*, *339*, 104–114, doi:10.1016/j.sedgeo.2016.04.001

Quiring, S., A. Schumacher, C. Labosier, and L. Zhu (2011), Variations in mean annual tropical cyclone size in the Atlantic, *J. Geophys. Res.*, *116*, D09114, doi:10.1029/2010JD015011.

Roeber, V., and J. D. Bricker (2015), Destructive tsunami-like wave generated by surf beat over a coral reef during Typhoon Haiyan, *Nat. Commun.*, *6*, 7854, doi:10.1038/ncomms8854.

Sawai, Y., et al. (2009), Aperiodic recurrence of geologically recorded tsunamis during the past 5500 years in eastern Hokkaido, Japan, *J. Geophys. Res.*, *114*, B01319, doi:10.1029/2007JB005503.

Sekimoto, T., K. Simizu, Y. Kubo, S. Imai, and M. Shimazu (1990), Field survey according to generation and propagation of surf-beat inside and outside of harbor, *Proc. Coastal Eng. Jpn. Soc. Civ. Eng.*, *37*, 86–90.

Shaw, J., Y. You, D. Mohrig, and G. Kocurek (2015), Tracking hurricane-generated storm surge with washover fan stratigraphy, *Geology*, *43*, 127–130, doi:10.1130/G36460.1.

Shimozono, T., Y. Tajima, A. B. Kennedy, H. Nobuoka, J. Sasaki, and S. Sato (2015), Combined infragravity wave and sea-swell runup over fringing reefs by super typhoon Haiyan, *J. Geophys. Res. Oceans*, *120*, 4463–4486, doi:10.1002/2015JC010760.

Soria, J., A. D. Switzer, C. L. Villanoy, H. M. Fritz, P. H. T. Bilgera, O. C. Cabrera, F. P. Siringan, Y. Y. Maria, Y., R. D. Ramos, and I. Q. Fernandez (2016), Repeat storm surge disasters of Typhoon Haiyan and its 1897 predecessor in the Philippines, *Bull. Am. Meteorol. Soc.*, *97*, 31–48, doi:10.1175/BAMS-D-14-00245.1.

Sugawara, D., T. Takahashi, and F. Imamura (2014), Sediment transport due to the 2011 Tohoku-oki tsunami at Sendai: Results from numerical modelling, *Mar. Geol.*, *358*, 18–37, doi:10.1016/j.margeo.2014.05.005.

Switzer, A. D., J. L. A. Soria, M. Manglicmot, A. Gallentes, and F. Siringan (2014), Boulder fields on Samar island, Philippines deposited by super typhoon Haiyan: Implications for the storm vs tsunami debate, in *Proceedings of 2014 GSA Annual Meeting in Vancouver, British Columbia* (19–22 Oct 2014). [Available at https://gsa.confex.com/gsa/2014AM/finalprogram/abstract_245723.htm.]

Szczuciński, W. (2012), The post-depositional changes of the onshore 2004 tsunami deposits on the Andaman Sea coast of Thailand, *Nat. Hazards*, *60*, 115–133, doi:10.1007/s11069-011-9956-8.

Tajima Y., et al. (2014), Initial report of JSCE-PICE joint survey on the storm surge disaster caused by typhoon Haiyan, *Coast. Eng. J.*, *56*, doi:10.1142/S0578563414500065.

Tajima, Y., T. Shimozono, K. H. Gunasekara, and E. C. Cruz (2016a), Study on locally varying inundation characteristics induced by super Typhoon Haiyan. Part 2: Deformation of storm waves on the beach with fringing reef along the east coast of eastern Samar, *Coastal Eng. J.*, *58*, doi:10.1142/S0578563416400039.

Tajima, Y., K. H. Gunasekara, T. Shimozono and E. C. Cruz (2016b), Study on locally varying inundation characteristics induced by super Typhoon Haiyan. Part 1: Dynamic behavior of storm surge and waves Around San Pedro Bay, *Coastal Eng. J.*, *58*, doi:10.1142/S0578563416400027.

Takagi, H., M. Esteban, T. Shibayama, T. Mikami, R. Matsumaru, M. De Leon, N. Thao, T. Oyama, and R. Nakamura (2017), Track analysis, simulation, and field survey of the 2013 Typhoon Haiyan storm surge, *J. Flood Risk Manage.*, *10*, 42–52, doi:10.1111/jfr3.12136.

Takeuchi H., Y. Murashima, F. Imamura, N. Shuto, and K. Yoshida (2005), Verification of tsunami run-up height records of Meiji Sanriku Tsunami and Showa Sanriku Tsunami on the coast of Iwate Prefecture using numerical simulation, *Hist. Earthq.*, *20*, 155–163.

The Ministry of Agriculture, Forestry and Fisheries (2015), *Guideline to Make Assumption Area Map Inundated by Storm Surge*. [Available at http://www.maff.go.jp/j/press/nousin/bousai/pdf/150721-02.pdf.]

TPXO (2014), *The OSU TOPEX/POSEIDON Global Inverse Solution*. [Available at http://volkov.oce.orst.edu/tides/global.html.]

U.S. Agency for International Development (2014), *Philippines Tphyoon Yolanda/Haiyan Fact Sheet #21*.

Williams, H. F. (2013), 600-year sedimentary archive of hurricane strikes in a prograding beach ridge plain, southwestern Louisiana, *Mar. Geol.*, *336*, 170–183, doi:10.1016/j.margeo.2012.12.005.

Williams, H. F. (2015), Contrasting styles of Hurricane Irene washover sedimentation on three east coast barrier islands: Cape Lookout, North Carolina; Assateague Island, Virginia; and Fire Island, New York, *Geomorphology*, *231*, 182–192, doi:10.1016/j.geomorph.2014.11.027.

Yamada, M., S. Fujino, and K. Goto (2014), Deposition of sediments of diverse sizes by the 2011 Tohoku-oki tsunami at Miyako City, Japan, *Mar. Geol.*, *358*, 67–78, doi:10.1016/j.margeo.2014.05.019.

Yi, C. J., A. Suppasri, S. Kure, J. D. Bricker, E. Mas, M. Quimpo, and M. Yasuda (2015), Storm surge mapping of Typhoon Haiyan and its impact in Tanauan, Leyte, Philippines, *Int. J. Disaster Risk Reduct.*, *13*, 207–214, doi:10.1016/j.ijdrr.2015.05.007.